Available online at www.sciencedirect.com
ScienceDirect
Continental Shelf Research 26 (2006) 2393–2414
CONTINENTAL SHELF RESEARCH
www.elsevier.com/locate/csr

Direct observations of a medium-intensity inflow into the Baltic Sea

Jürgen Sellschopp[a,*], Lars Arneborg[b], Michaela Knoll[a], Volker Fiekas[a], Frank Gerdes[a], Hans Burchard[c], Hans Ulrich Lass[c], Volker Mohrholz[c], Lars Umlauf[c]

[a]*FWG, Klausdorfer Weg 2-24, D-24148 Kiel, Germany*
[b]*Department of Oceanography, Göteborg University, Guldhedsg. 5A, Box 460, SE-40530 Göteborg, Sweden*
[c]*Baltic Sea Research Institute Warnemünde, Seestr. 15, D-18119 Rostock-Warnemünde, Germany*

Received 21 April 2006; received in revised form 28 June 2006; accepted 12 July 2006
Available online 12 September 2006

Abstract

In January/February 2004 a ship cruise into the Arkona Sea (Western Baltic) happened to start just prior to a medium-size inflow event and to last until a few days after the inflow. The bottom layer of saline inflow water in the southern Sound has a current speed of up to 1 m/s. The current bifurcates at Kriegers Shoal, where only the smaller branch follows the contour lines of the bathymetry at the western rim of the basin, while the main flow proceeds on the steepest path north of Kriegers Shoal. The pycnocline tilt due to geostrophy matches with current observations in both branches. Old bottom water in the basin is lifted up by the denser inflow and pushed forward to Bornholm Gate. Inflow from the Darss Sill at first consists of low-salinity Baltic surface water and a small amount of higher salinity water at the bottom. After a few days the water over the sill is mixed and moves east, establishing a strong subsurface current at the southern rim of the Arkona Basin. Neither the inflow through the Sound nor the water masses from the Darss Sill reached the Bornholm Gate in the east of the Arkona Sea before the end of the survey. The saline outflow observed there consists of bottom water that had been present in the Arkona Sea prior to the new inflow. Overflow water spreading on the sea bottom is modified by entrainment from the low salinity water body above. Best guesses of the entrainment rate, somewhat tentative due to salinity variations at the entrance, are in line with formulae from the literature.

Keywords: Marginal seas; Inflow; Water masses; Water mixing; Salinity stratification; Baltic Sea

1. Introduction

The Baltic Sea is connected with the world ocean via a topographically complex system of straits and basins. Its water is brackish due to freshwater surplus and water exchange through straits. The halocline on top of the invaded water, which rests in the basins of the Baltic and deserves the attribute "highly saline" only in comparison with Baltic surface water, is associated with a strong density contrast which prevents wind mixing and deep convection in winter. Sufficiently frequent inflows of ample quantities of Kattegat water are able to

*Corresponding author. Tel.: +49 341 607 4118; fax: +49 4307 839237.
E-mail addresses: jsellschopp@bwb.org (J. Sellschopp), laar@oce.gu.se (L. Arneborg), hans.burchard@io-warnemuende.de (H. Burchard).

0278-4343/$ - see front matter © 2006 Elsevier Ltd. All rights reserved.
doi:10.1016/j.csr.2006.07.004

compensate for the continuous decrease of oxygen in the bottom layers of the basins. Therefore, unlike the Black Sea with its limited inflow of high salinity water through the Bosporus, the Baltic Sea has no permanent anoxic regions but only occasional pools filled with hydrogen sulphide, when the oxygen is temporarily consumed. The importance of salt water inflows into the Baltic drives thoroughgoing research of exchange mechanisms and the assessment of enhanced mixing by man-made obstructions.

Seventeen days of ship time were available in winter 2004 for a research cruise into the Arkona Sea, the first basin of the Baltic Sea passed by any inflow of haline water. The main instrumentation consisted of an SBE 911plus CTD package, a vessel mounted 600 kHz workhorse Acoustical Doppler Current Profiler (ADCP), a towed CTD chain and a microstructure turbulence profiler. We describe in this work the observations before, during and after a medium-size inflow event, which was observed for the first time. Part of the results was presented in an early paper on idealized numerical modelling of plume dynamics (Burchard et al., 2005) and in a recent paper on gravity current dynamics and entrainment (Arneborg et al., 2006).

Fig. 1 shows the locations of 273 CTD stations, 310 km CTD chain tow tracks and permanent monitoring stations (RDANH, 2004; BSH, 2005; SMHI, 2006), the data of which were complementarily used. The paper is organized in accordance with the temporal stages of salt water inflow into the Arkona Sea. Section 2 describes the general situation in the Arkona Sea and the conditions prior to the inflow. In Section 3 the volume transport through the Sound is calculated from sea level height at four coastal stations. The spreading of inflow water in the Arkona Basin is the subject of Section 4, while Section 5 sets a spotlight on the flow north of Kriegers Shoal. Observations of water masses that arrived from the Darss Sill are presented in Section 6. Finally, the outflow of bottom water through Bornholm Gate is shown in Section 7, before we conclude in Section 8.

2. Conditions in the Arkona Sea prior to the inflow

The Arkona Sea, with an area of 18673 km^2, a volume of 432 km^3 and a maximum depth of 45 m (Ehlin et al., 1974), is located at the entrance of the central Baltic. All water masses exchanging between the North Sea and the central Baltic must pass the Arkona Sea, the westernmost basin of the Baltic Proper. More than 70% of the volume transport crosses the 18 m deep Darss Sill and runs through the Danish Belts and the Belt Sea in the west (Jacobsen, 1980). The rest passes the 8 m deep Drogden Sill in the southern part of the Sound. The long-term mean water exchange consists of an outflow of 30,000 m^3/s of Baltic surface water with average salinities of 8.5 and an inflow of 15,000 m^3/s of water from the Kattegat with average salinities of 17 maintaining the overall salt content in the Baltic. Short-term characteristics of the water exchange are nevertheless quite variable both with respect to salinity and volume flow (Liljebladh and Stigebrandt, 1996).

The exchange on time scales of days and weeks is predominantly barotropic. It is driven by sea level differences which are caused by the wind field. Westerly winds increase the sea level in the Kattegat and decrease it in the western part of the Baltic Sea causing an inflow of saline water (Matthäus and Franck, 1992). Only an exceptionally strong inflow is able to reach and modify the bottom layer in the Gotland Basin. Major inflows were defined by Matthäus and Franck (1992) via the presence of high salinity water from bottom to surface at Gedser Rev lightvessel. After a 15 year period of steady deepwater temperature in the Gotland Basin, a major inflow was observed in January 2003 that renewed most of the deep water in the central Baltic (Feistel et al., 2003). Additionally exceptional warm water inflows, which do not meet the surface salinity criterion of Matthäus and Franck (1992), occurred in the summers 2002 and 2003, the latter of which was able to raise the temperature in the Gotland Sea (Feistel et al., 2004). Generally, major inflows occur on inter-annual time scales while medium-intensity inflow events, which fill the Arkona and Bornholm Basins, may happen several times a year.

A medium-intensity inflow event, which pushed 18% of the yearly amount of saline Sound water over the Drodgen Sill, started end of January 2004. In the evening of February 1 the plume front arrived at Falsterborev (see Fig. 1 for all locations). The hydrographic conditions in the Arkona Sea prior to that inflow event were sampled through CTD stations and a CTD chain tow path (marker symbols and continuous tracks in Fig. 1). Data show the typical stratification during winter time. Salinities between 7.8 and 8.8 were observed in the surface layer while the highest values of more than 18 were recorded at the bottom in the northern part

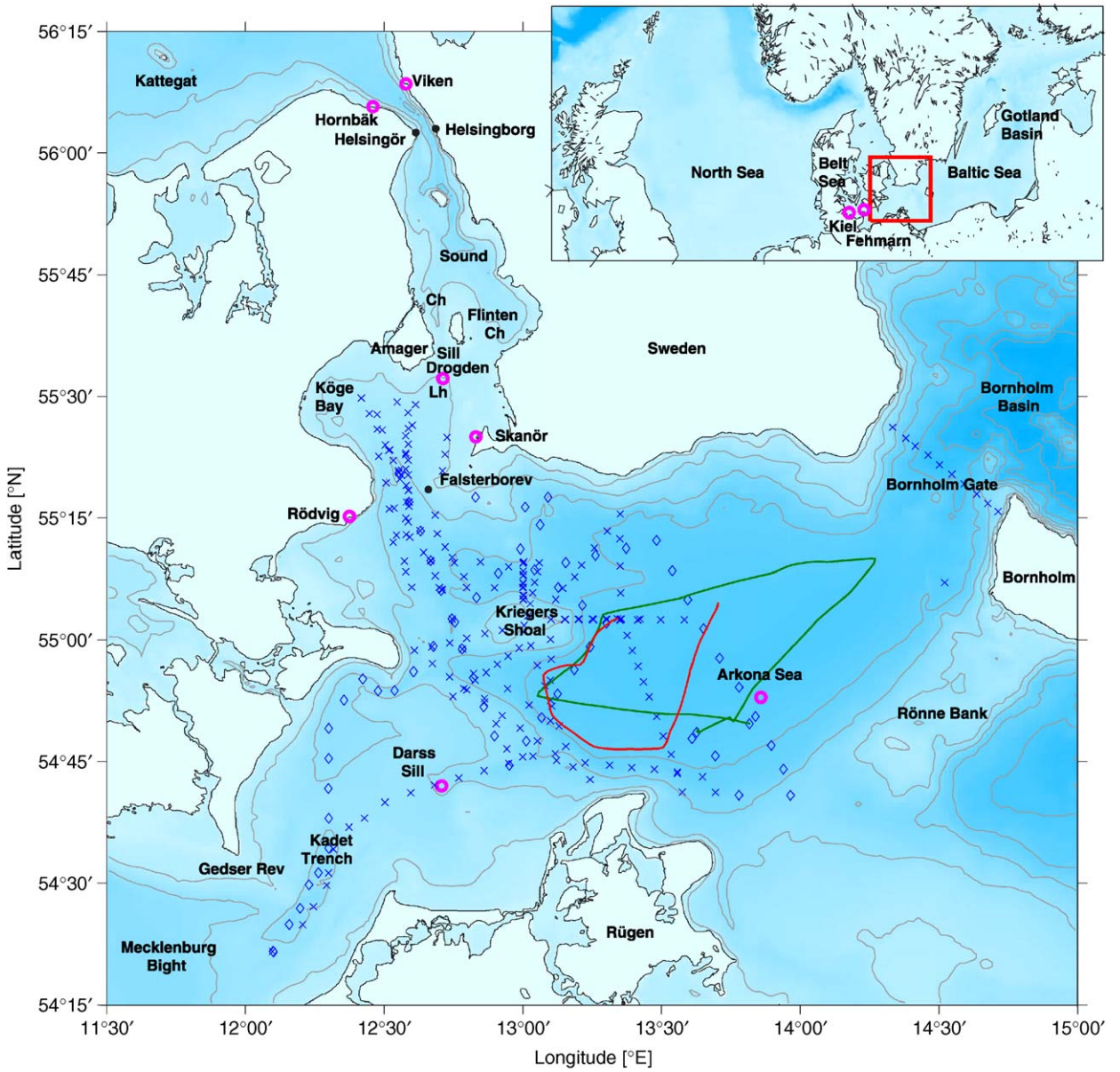

Fig. 1. Topography of the Arkona Sea with bathymetry lines every 10 m, fixed monitoring stations (bold line rings), CTD stations before (diamonds) and after (crosses) the inflow event, towed CTD-chain tracks before (closed loop) and after (*U*-shaped) the inflow event.

of the Arkona Basin. The temperature at the surface was 2–3 °C except for marginal locations where temperatures as low as 1 °C were observed. The water column was mostly well mixed in the upper layer. Between 15 m depth and the main halocline at 38 m, thermohaline fine structure was present with temperatures between 2 and 4 °C and salinities below 11 (Fig. 2). In the trenches north and southeast of the Darss Sill, the bottom salinity reached 15 at 25 m depth, though. The most saline water at the bottom of the Arkona Basin had temperatures in excess of 6 °C. The 40 m long towed CTD-chain could hardly touch the thin saline bottom layer. The doming of the isopycnals observed in the eastern CTD-section at about 55°N and in the CTD-chain section between 13°30′ and 13°45′E (Fig. 2) was caused by cyclonic eddies which can be seen in the current field of the upper layer obtained by the vessel-mounted ADCP (Fig. 3). Similar eddies and the corresponding

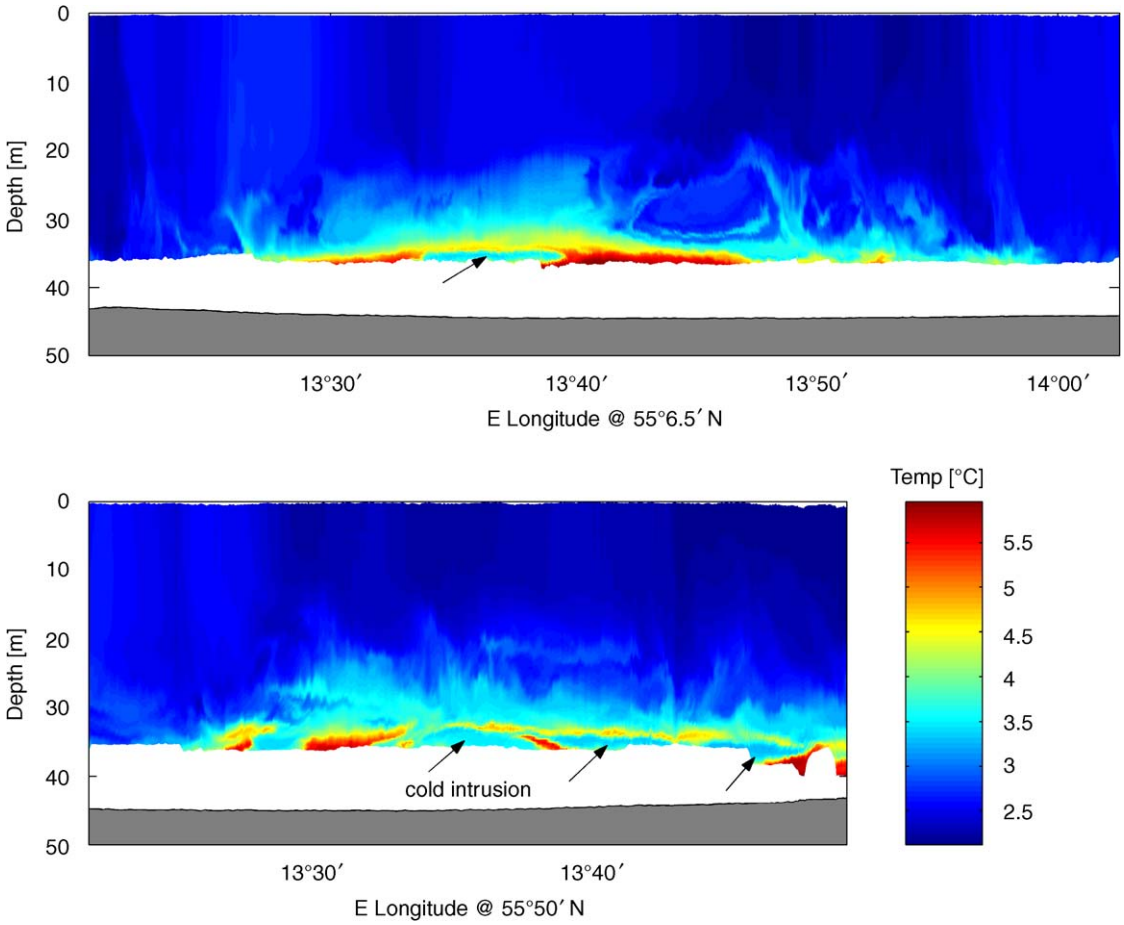

Fig. 2. Temperature sections of the CTD chain on January 29 and 30 prior to the inflow event. The residual saline bottom layer is hardly touched by the towed instrument except where the interface is uplifted in two cyclonic eddies (see Fig. 3). A cold intrusion, indicated by arrows, is present in the halocline at 35 m depth.

upwelling of isohalines were observed in earlier measurements (Lass and Mohrholz, 2003) and seem to be typical for that area.

3. Inflow through the Sound

Saline inflows through the Danish Belts and the Sound (Fig. 1) are generally barotropic over the shallowest sill regions, where the pressure gradient caused by surface elevation differences is balanced by bottom friction and form drag. The surface elevation differences are caused by regional wind patterns (Gustafsson and Andersson, 2001). Westerly winds tend to raise the Kattegat sea level and lower the Arkona Sea level, thereby causing inflows, whereas easterly winds tend to cause outflows. The frictional balance has been confirmed by several studies (e.g. Jakobsen et al., 1997, Green and Stigebrandt, 2002), which have shown that the flow through the Sound can be well described by a quadratic friction law of type

$$H_N - H_S = KQ|Q|, \quad (1)$$

where $H_N - H_S$ is the total head difference from south to north, which is taken to be equal to the water level difference, Q is the southward volume flux, and K is the specific resistance. Jakobsen et al. (1997) estimated the volume fluxes from ADCP measurements from the Drogden and Flinten channels, and used sea level data from Hornbäk and Viken to the North and Rödvig and Skanör to the south. They found the average value for the specific resistance to be $K = 226 \times 10^{-12}\,\mathrm{s^2\,m^{-5}}$. This value is used to calculate the volume fluxes from observed sea level differences between Viken and Skanör for the last half of January and the first part of February 2004 (Fig. 4).

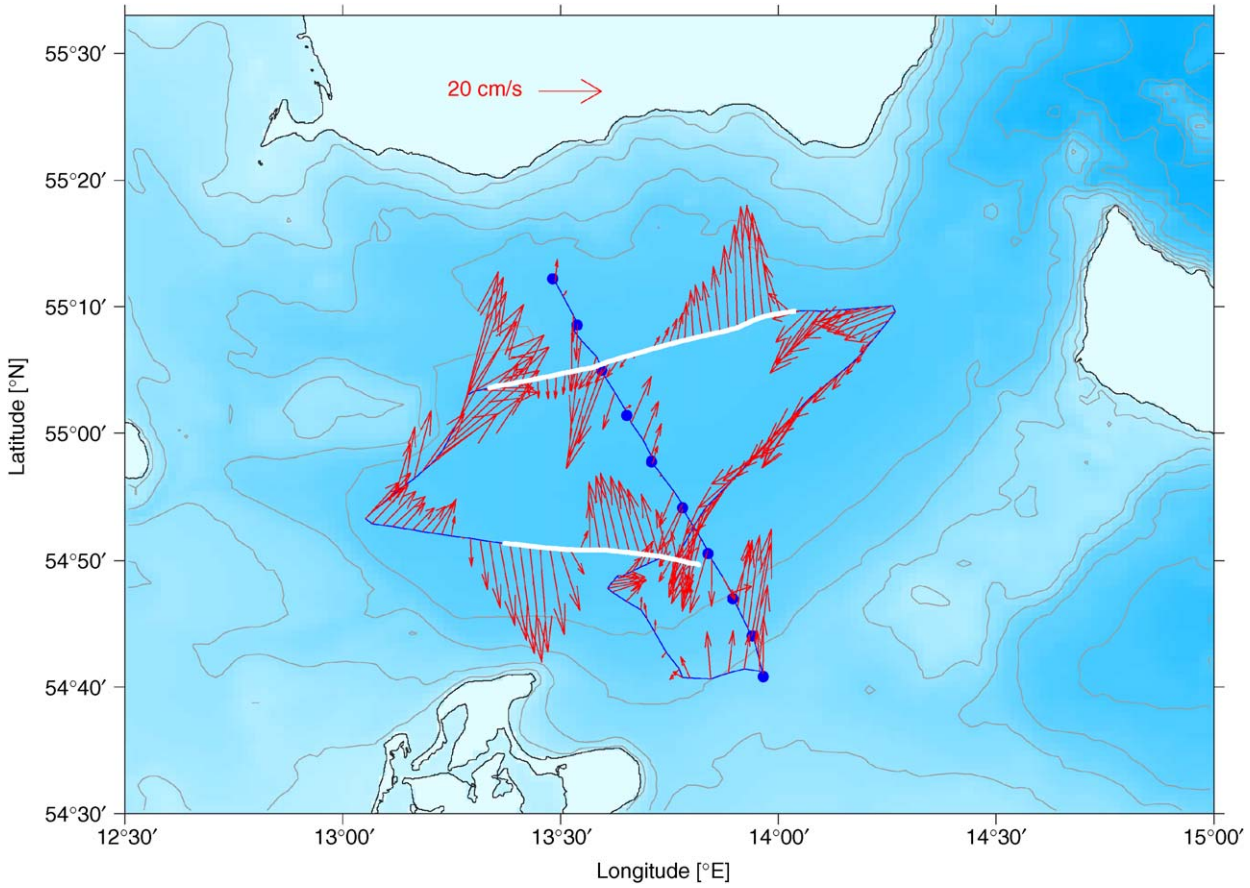

Fig. 3. Current field averaged over 10 min and 10–15 m depth from January 29, 2004 0:30 h to January 30, 2004 9:00 h. Bold lines denote the sections of Fig. 2. At the northern intersection the time difference of one day between the CTD track and the CTD chain track must be considered.

During the last half of January 2004 winds were variable, causing no prolonged inflows or outflows through the Sound (Fig. 4). Remainders of previous overspills had sufficient time to leave through the southern exit of the Sound. Bottom salinity exceeding 11 was nowhere found between Drogden and Kriegers Shoal. On January 26, the winds turned to westerly directions at about $10\,m\,s^{-1}$ and remained in westerly directions until February 11. The flows through the Sound reacted directly on the new wind field and became predominantly southward, which is clearly seen in the cumulated inflow curve. On February 1, a saline plume extending about 30 km south of the Sound was observed moving southward.

4. Spreading of saline Sound water

The Royal Danish Administration of Navigation and Hydrography (RDANH) maintains an oceanographic observation post at Drogden lighthouse. Because of topographic effects currents measured at Drogden lighthouse cannot be directly translated into volume flux. In fact the average current in January/February 2004 at Drogden lighthouse sets towards ESE, which is very different from the gross direction of the Sound. Nevertheless, the accumulated northern current components measured at several depths (lower panel of Fig. 4) compare well with volume fluxes calculated from water level differences. The match was obtained by multiplication of the accumulated northern current components with $0.08\,km^2$, which is the approximate cross-section of the Sound from the southern tip of Amager to the Swedish coast (see Fig. 1). For the opposite flow direction a slightly larger cross-section is required for an optimal match.

Continuous salinity measurements at Drogden lighthouse which would complement the current records and provide the best possible estimate of the

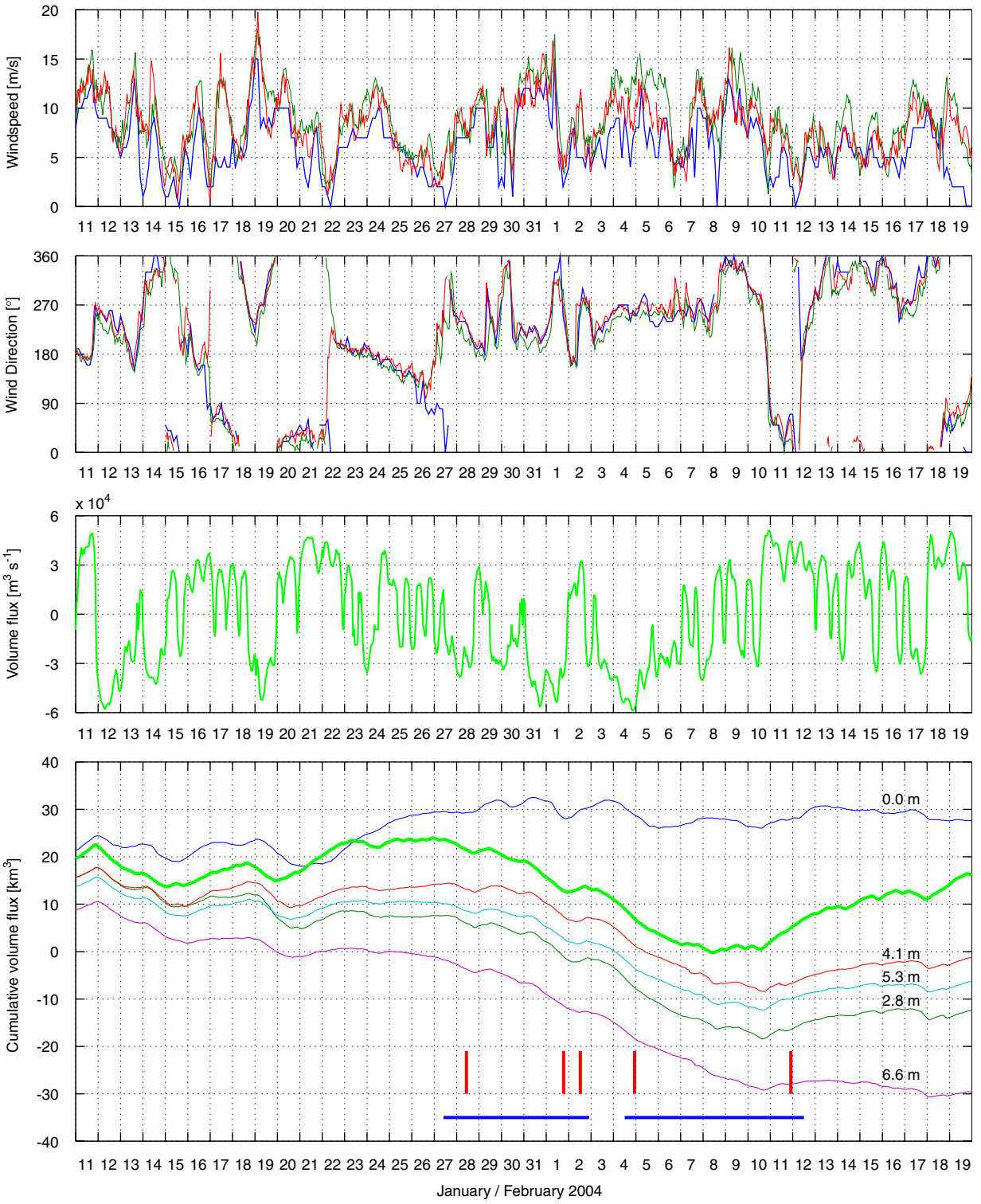

Fig. 4. Time series of wind speed, wind direction from the Darss Sill Station (red), the Arkona Sea Station (green), and from Falsterbo (blue), and northward volume fluxes calculated from observed sea levels at Viken and Skanör (Fig. 1) using (1). Thin lines in the last panel are accumulated northward currents at Drogden lighthouse at different depths multiplied by a 0.08 km^2 cross-section. The bold curve is accumulated volume flux from the panel above. Horizontal bars at the bottom of the panel indicate two phases of the cruise. The instants of time when CTD sections in the southern Sound were obtained (Fig. 5) are marked by five vertical bars.

saltwater inflow from the Sound did unfortunately not start before March 2004. CTD casts in the southern Sound are used instead for the characterization of the water masses arriving from the Drogden channel.

Five CTD sections (Fig. 5) from visits of the southern Sound within 15 days are marked in Fig. 4. When the water masses south of Drogden lighthouse were for the first time assessed on January 28 (first panel of Fig. 5), the flow in the Sound had just turned south and no Kattegat water had yet passed the Drogden Sill. Maximum salinity of the thin bottom layer was below 12. Four days later on February 1 (second panel of Fig. 5) Kattegat water with salinity between 19 and 21 was met everywhere north of Falsterborev (55°20′N). Close to the island of Amager (55°30′N) modified Kattegat water was found at the surface, further south it was covered by low-salinity Baltic water and was spilling downhill in a bottom layer of more than 5 m thickness. The average southward current component in that layer is 0.5 m/s, identical to that at Drogden lighthouse. The volume of saline inflow water, which is present in the southern part of the Sound, is 2 km^3 at most, while three to four times that quantity must have passed the Drogden Sill between January 28 and February 1 (Fig. 4), most of which has gone into the deeper Arkona Basin. Taking into consideration the intermittency of the inflow it seems obvious that the plume front near Falsterborev in Fig. 5 (second panel) originates from the last peak flow at some time between January 31 and February 1 rather than from the beginning of the inflow.

Between the sections of February 1 and February 2 (second and third panel of Fig. 5) no additional Kattegat water had passed the Drogden Sill. During these 18 h the plume front progressed by about 18 km. The mean frontal velocity of 27 $cm\,s^{-1}$ is similar to the current velocity of the bottom layer on February 2. In the southern Sound the bottom layer has largely been drained into the Arkona Basin. The Baltic water which is now filling most of the water column moves north into the Drogden and Flinten channels.

Within the next 58 h from February 2 to 4, the inflow from the Sound of 6 km^3 causes a strong southward current and a pycnocline rise in the southern Sound to at least mid-depth (fourth panel of Fig. 5). The inflow period ends on February 7 and is followed by $3\frac{1}{2}$ days of changing flow directions. When the CTD section of February 11 (fifth panel of Fig. 5) was taken, the flow had reversed to north for $1\frac{1}{2}$ days already. A more than 5 m thick layer of saline bottom water is left in the southern Sound flowing south, while the Baltic surface water goes north.

The path of the salty and dense Kattegat water after it leaves the Sound has been under discussion (Lass et al., 2002, 2005; Burchard et al., 2005). Since gravity, the Coriolis force, bottom friction and the peculiarities of the bottom topography altogether control the pathway of a dense plume, it is not a priori clear which direction the plume might take. Whether it tends to follow the isolines of the bathymetry and encircles the basin or proceeds to depth almost directly along the steepest path, may also depend on the volume of the plume.

On February 5, when the inflow from the Sound was fully developed, a CTD section across two channels near Kriegers Shoal (Fig. 6) was taken. The direct path to the deepest basin runs north of Kriegers Shoal, but a geostrophically balanced current would rather pass through the gap between Kriegers Shoal and the western sill. Although at depths greater than 22 m part of the data from the 600 kHz ADCP did not pass the quality control, the streams of inflow water leaning at the sloping bottom on their right are clearly visible in Fig. 6. In that figure, the area below the salinity 11 contour line of the western branch is less than half the area of the northern branch. Considering the lower average salinity in the western branch, the likely lower current speed, and the projection of the current onto the plane of the section, the amount of inflowing water passing Kriegers Shoal in the west is likely to be much smaller than the flow north of Kriegers Shoal.

Four days after the end of the inflow period, on February 11, when the remainders of Kattegat water were running down from the shallow southern Sound, both trenches were crossed again (Fig. 7). In the narrow channel west of Kriegers Shoal the speed of the saline water is about 20 $cm\,s^{-1}$, while the current speed in the bottom layer north of Kriegers Shoal is again unknown because of missing backscatter. There is thus no testimony for a higher quantity of saline water flowing through the northern branch. The density of the water in the western channel is not higher than that of the old bottom water in the Arkona Basin. The saltier inflow water north of Kriegers Shoal, however, is going to replace the old bottom layer in the basin.

Older bottom water in the Arkona Sea is distinguished from recent inflow water by its higher

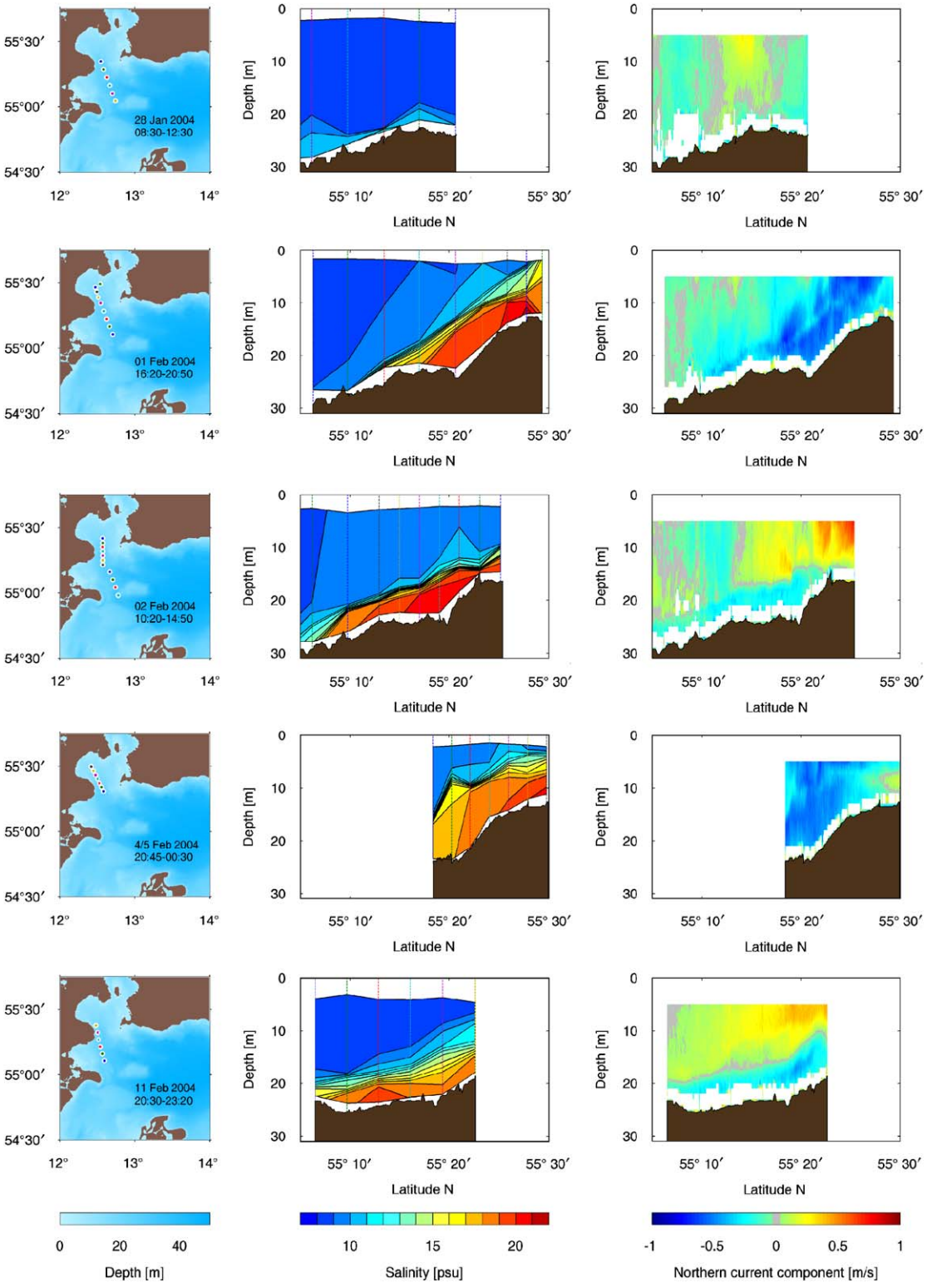

Fig. 5. Positions of CTD stations, salinity and northern current components in the southern Sound on January 28 (first panel), on February 1 (second panel), on February 2 (third panel), on February 4 (fourth panel), on February 11 (fifth panel). Dates of the sections are indicated in Fig. 4.

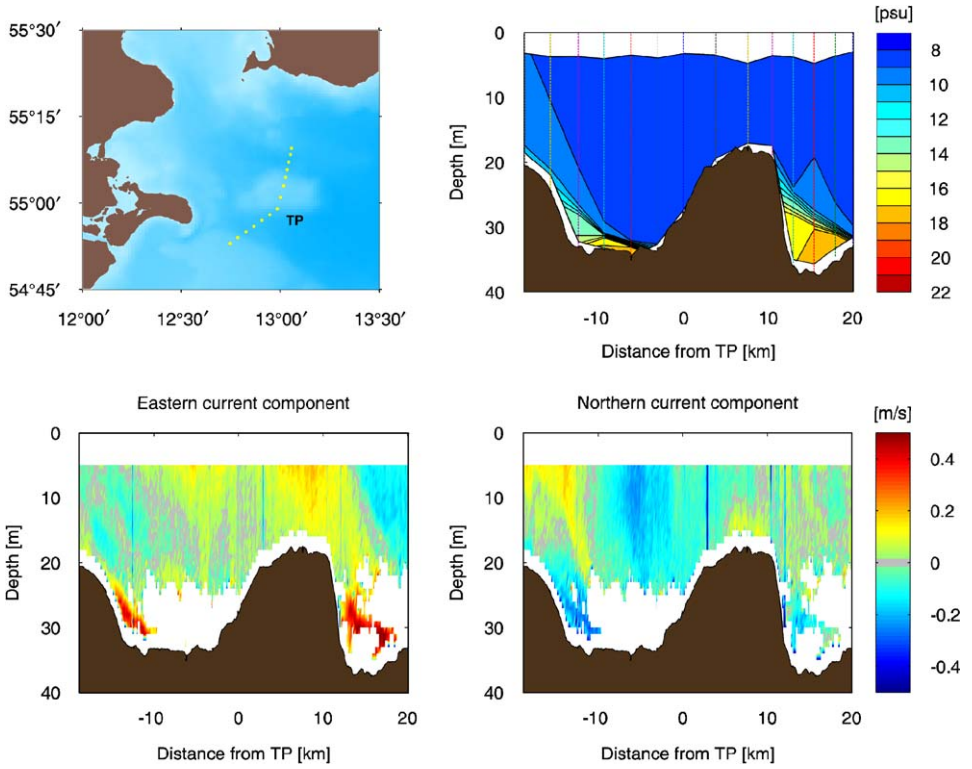

Fig. 6. Section across Kriegers Shoal on February 5. Upper left: position of CTD stations, upper right: salinity section, lower left and right: eastern and northern current components obtained by the ship-borne ADCP. Data gaps at larger water depth are due to insufficient backscatter of the pings. The 600 kHz RDI workhorse was set up for 64-depth cells of size 1 m, one water column and one bottom track ping per ensemble, bottom track mode 5, maximum tracking depth 125 m, salinity 10, wide bandwidth, ambiguity velocity 3.6 m s^{-1}, time per ensemble 1 s, time between pings 0.59 s, radial beam coordinates. All ADCP plots were made from short-term averages over half minutes, i.e. 22 or 23 pings.

temperature, 5–6 versus 3–4.2 °C at salinities above 15. Cold water did exist below the surface layer prior to the inflow event, but with salinity between 10 and 15 it formed an intrusion layer in the halocline. It was sensed at essentially every CTD station taken on at least 40 m water depth and showed up even in the CTD chain tow of January 29 and 30 (Fig. 2), when two cyclonic eddies doming up the interface were cut by the track (see Fig. 3). Outside the eddies the cold intrusion was out of reach of the towed chain, which had to be kept at safe distance from the bottom. In the February measurements, after the new saline water had started to spill into the Arkona Basin, no sign of the deep cold intrusion was left over. The new saline inflow from the Sound is denser than the old warmer bottom layer and spreads directly on the bottom.

The old bottom water is lifted up by the underflow of new saline water or it is pushed forward towards the exit of the basin. Fig. 8 gives an estimate of the spreading of the new inflow water and the recession of the old warmer bottom water as derived from CTD stations and a CTD chain tow between February 4 and 8. On February 11, the inflow has reached the centre of the basin. Old bottom water is still present next to the bottom layer on most CTD stations in a section east of Kriegers Shoal. Property and thickness of the old bottom water layer vary similarly to the towed chain measurements in Fig. 2.

5. Conditions north of Kriegers Shoal

5.1. Dynamics

Four times during the inflow, cross-sections with ADCP and several CTD stations were carried out north of Kriegers Shoal. The three last sections (Figs. 9 and 7) were performed on the 13°E

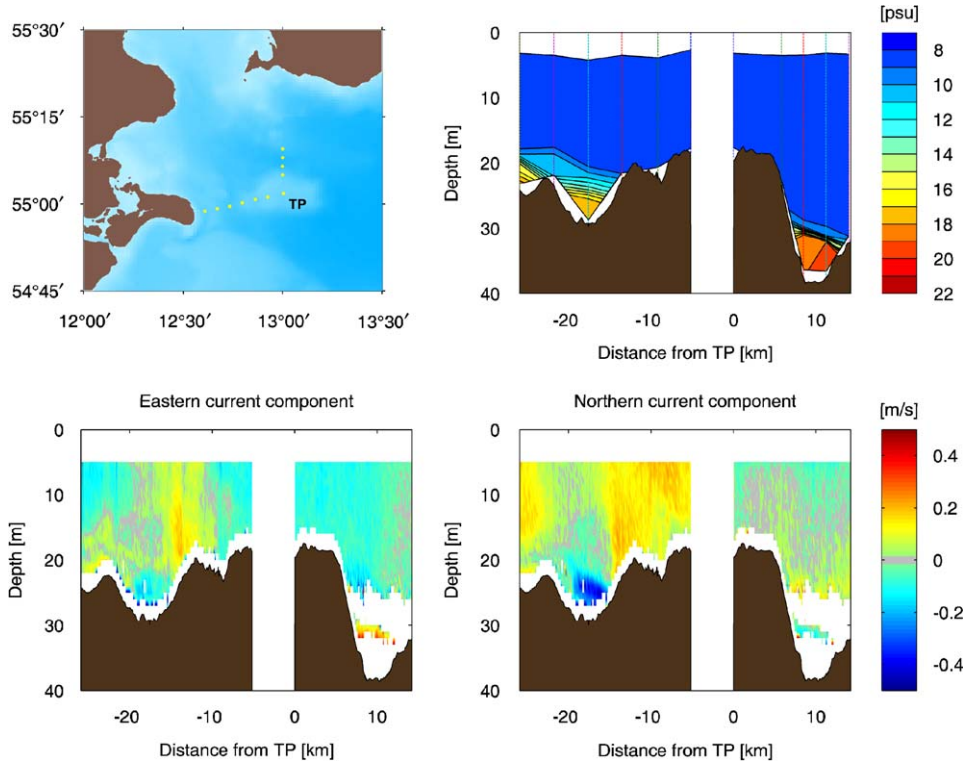

Fig. 7. Sections across the trenches west and north of Kriegers Shoal on February 11. Upper left: position of CTD stations, upper right: salinity section, lower left and right: eastern and northern current components obtained by the ship-borne ADCP. Data gaps at higher water depth are due to insufficient backscatter of the 600 kHz pings.

meridian while the first (Fig. 6) was positioned a little further east (see Fig. 1). The salinity sections clearly show that the saline bottom layer leans against Kriegers Shoal to the south, as one would expect from geostrophy. This is also seen in the velocity sections although these do not cover the whole water column due to low backscatter amplitude. The salinities increase from about 17 on February 5 to 18 on February 6 to a maximum of 21 on February 7, and decrease to 19 on February 11. In addition there is a transverse salinity gradient within the current in all sections with the most saline water to the north and less saline water to the south. One explanation for this is that Ekman veering close to the bottom transports the densest water towards the north while a return current further up transports less dense water towards south. A complementary explanation is that this secondary circulation enhances stability on the northern side and reduces it on the southern side, which means that mixing on the northern side is reduced relative to that on the southern side. The thickness of the current is slightly increasing towards 10 m on February 7 with a decrease to about 7 m on February 11. The eastward velocities show a maximum core of about $0.5\,\mathrm{m\,s^{-1}}$ in the upper and central parts of the current, gradually decreasing towards the sides and the bottom of the channel.

The geostrophic eastward velocities can be calculated by integrating the thermal wind equation

$$\partial U/\partial z = g/(f\rho_0) \times \partial\rho/\partial y \tag{2}$$

with respect to z. Here, we follow the convention that the coordinates x and y (with corresponding velocities U and V) point towards the east and the north, respectively, and the z-axis upward. The integration has been performed by calculating the horizontal density gradient from the two deepest CTD profiles in each of the four sections, with the unknown integration constant being determined by fitting the geostrophic velocities to the observed velocities at 10 m depth, i.e. well above the bottom current. The geostrophic velocities are compared with the average eastward ADCP velocities between the two CTD stations in Fig. 10. Although there is

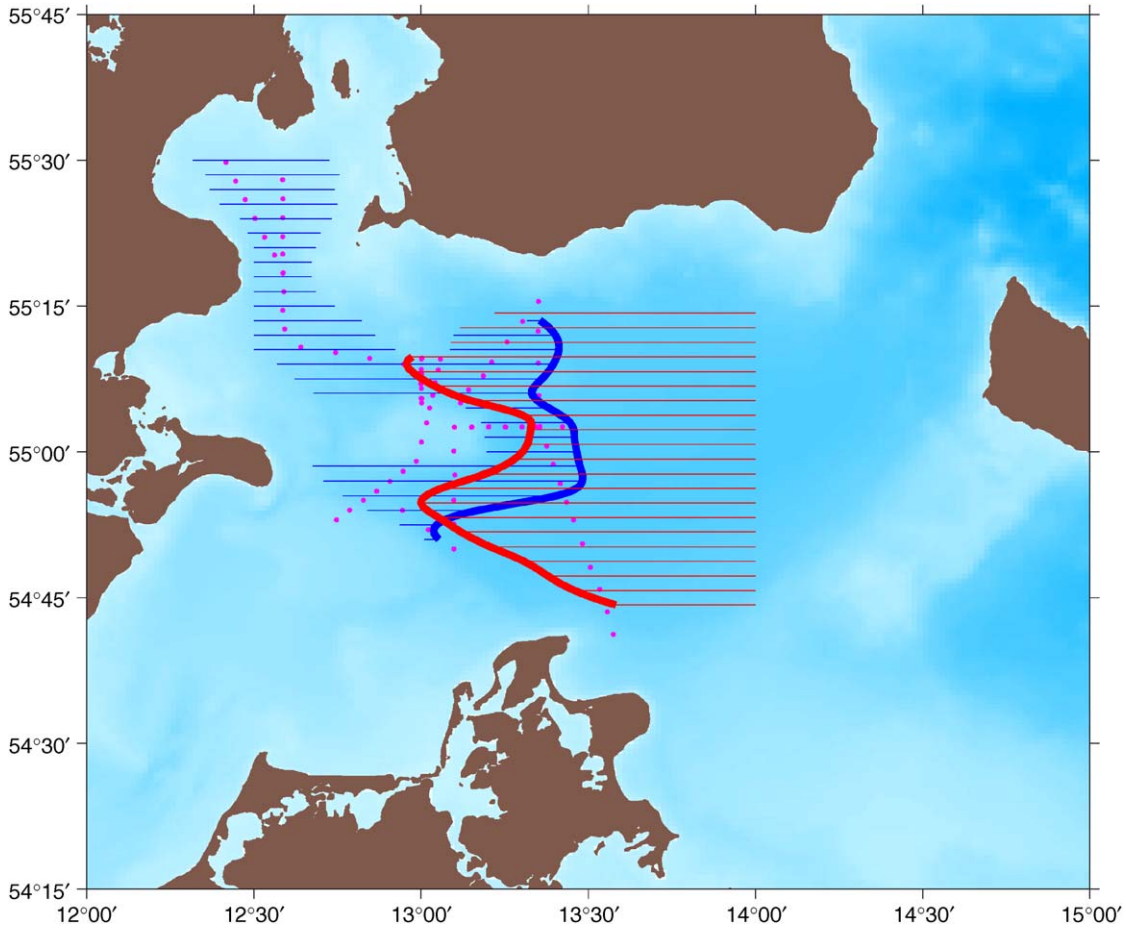

Fig. 8. Bottom water in the Arkona Basin on February 4–8, 2004. Dots indicate CTD stations during that period. The eastern bold line describes the front of the cold saline water proceeding from the Sound. The western bold line is the retreat line of old warmer bottom water. In the overlap area between 13°E and 13°30′E the new saline inflow has crept below the old bottom layer.

some scatter in the observed velocities due to problems with bad backscatter, the correspondence between the geostrophic and observed velocities is good. This means that the flow is in geostrophic balance in the cross-stream direction. One clear feature of the geostrophic velocities, which is also seen in some of the observed velocities, is a decrease in velocity with depth below the interface. This purely inviscid vertical shear in the geostrophic velocities is caused by the transverse density gradient within the current. The real current is, however, also influenced by bottom friction shear, and the interplay between these two distinctly different types of shear is beyond the scope of this paper.

The volume fluxes of saline water north of Kriegers Shoal are difficult to determine exactly due to the gaps in our ADCP data, but a rough estimate can be obtained by multiplying a representative velocity with the cross-sectional area of the gravity current. The cross-sectional area below the salinity 12 isoline is about 55 000–60 000 m^2 during the 5–7 February period and decreases to about 35 000 m^2 on February 11. With a representative velocity of about 0.4 $m\,s^{-1}$ this gives volume fluxes in the order of 23 000 $m^3 s^{-1}$ decreasing to 14 000 $m^3\,s^{-1}$ on February 11. These are reasonable numbers, when compared with the inflow volume fluxes through the Sound (Fig. 4), which vary between 0 and 50 000 $m^3\,s^{-1}$ during January 31–February 8, and decrease below 0 after that. This supports our findings given above that the main part of the water entering through the Sound follows a path north of Kriegers Shoal instead of continuing southward into the south-western Arkona Sea. The remaining volume of water

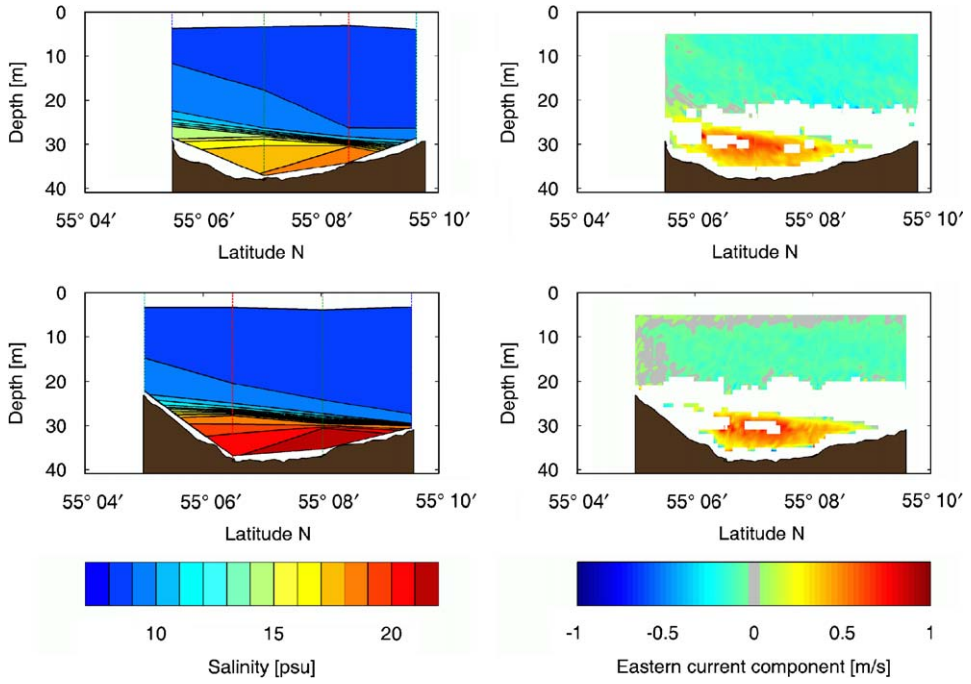

Fig. 9. Salinity and eastward velocity sections north of Kriegers Shoal on February 6 (upper panel) and February 7 (lower panel).

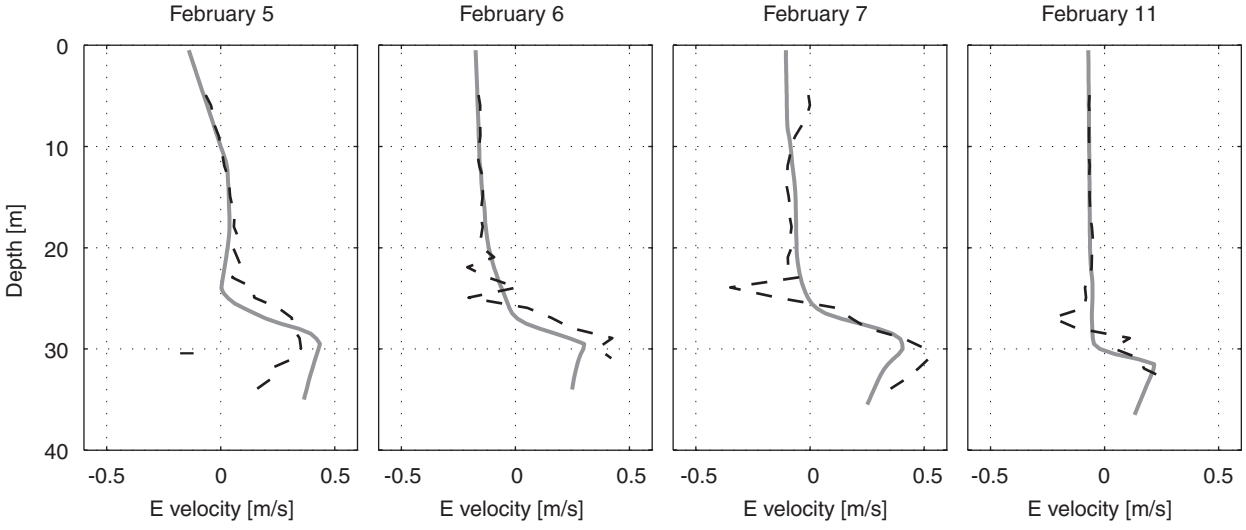

Fig. 10. Geostrophic (full) and observed (dashed) eastward velocities north of Kriegers Shoal on February 5–7 and 11.

flowing past Kriegers Shoal on February 11 must be the tail of the gravity current making its way down the hill after the inflow has stopped.

5.2. Entrainment

When a dense gravity current flows down a sloping bottom under the influence of gravity, Earth rotation, and bottom friction, ambient water is entrained into the current, reducing the density and increasing the volume flux of the current. For steep slopes and supercritical flows, the entrainment is a strong function of the Froude number,

$$Fr = U(g'h)^{-1/2}, \tag{3}$$

where U is the gravity current speed and h is its thickness. Observations of gravity currents with Froude numbers close to one indicate a dependency

of the form

$$w_E/U = 10^{-3}Fr^8 \quad (4)$$

(see Wåhlin and Cenedese, 2006 for a review), where w_E is the vertical velocity with which ambient water is entrained into the gravity current. Recent laboratory experiments of gravity currents on rotating gentle slopes (Cenedese et al., 2004) indicate a somewhat weaker dependency

$$w_E/U = 4 \times 10^{-4}Fr^{3.5}, \quad (5)$$

with the entrainment being caused by the breaking of roller waves on the interface. An alternative expression based on the along-flow slope rather than on the Froude number has been shown to work well for weak slopes and subcritical flows,

$$w_E/U = 0.07s, \quad (6)$$

where s is the bottom slope in the along-flow direction (Pedersen, 1980; Stigebrandt, 1987; Arneborg et al., 2004).

For a steady current, the entrainment can be found from the increase of volume flux or decrease in density or salinity in the flow direction. In our case the volume flux budgets are too unclear, but we should be able to see any entrainment effects in the salinity data. The salinity decreases in the flow direction as

$$\partial S/\partial x = (S - S_0)Bw_E/Q, \quad (7)$$

where S_0 is the salinity outside the gravity current, B is gravity current width, and Q is the volume flux.

In our data from north of Kriegers Shoal, we saw that the salinity varied considerably during the inflow period, which means that the current is not steady. The best we can get is a section of CTD profiles on February 4–5 starting in the Sound and ending north of Kriegers Shoal. The section time is about 18 h, while the advection time for the gravity current water is about 40 h, which means that the last profile was taken in water that entered through the Sound 22 h before the first profile. If we add the cross-section north of Kriegers Shoal on February 6 we obtain a time span of 42 h, which means that the last profiles at Kriegers Shoal should correspond to the first profiles in the Sound. The profiles are shown in Fig. 11. The shallowest profiles are from the Sound while the deepest are from north of Kriegers Shoal. The largest salinities are from Köge Bay and from a station west of the Kriegers Shoal section on February 5.

There is no strong trend in the salinity data. The most common bottom layer salinity seems to be about 17–18, and there is quite a lot of variability both in the Sound area and in the Kriegers Shoal area. However, there is a tendency of the Sound salinities to be concentrated around 18–19, while the Kriegers Shoal salinities are more concentrated around 17–18. With a salinity decrease of about 1 and a flow path length of about 80 km we obtain a salinity gradient in the order of $\partial S/\partial x = 1.3 \times 10^{-5}\,\mathrm{m}^{-1}$. With the other parameters in (7) being given by $S = 18$, $S_0 = 8$, $Q = 2.3 \times 10^4\,\mathrm{m}^3\,\mathrm{s}^{-1}$, and $B = 10\,\mathrm{km}$, we obtain an entrainment rate in the order of, $w_E = 3 \times 10^{-6}\,\mathrm{m\,s}^{-1}$.

With typical gravity current speeds of about 0.3–0.4 $\mathrm{m\,s}^{-1}$, thicknesses in the order of 5–10 m, and a reduced gravity of $g' = 0.08\,\mathrm{m\,s}^{-2}$, a representative Froude number for the current is $Fr = 0.4$–0.5. The predicted entrainment rates using (4) is in the range $w_E = 0.2$–$1.6 \times 10^{-6}\,\mathrm{m\,s}^{-1}$ which is quite a wide range and tends to underestimate the observed value. When using (5), the predicted entrainment rates fall in the range $w_E = 4.9$–$14 \times 10^{-6}\,\mathrm{m\,s}^{-1}$, which is more than observed. Finally, the bottom slope is about $s = 4 \times 10^{-4}$, which means that the entrainment rate predicted by (6) is $w_E = 8.4$–$11 \times 10^{-6}\,\mathrm{m\,s}^{-1}$, which is about a factor of 3 too large. So, generally the strongest Froude number dependency entrainment parameterization based on observations at larger Froude numbers tends to underestimate the present low Froude number entrainment rates, while the other two expressions tend to overestimate the entrainment rates. However, all expressions predict something within the correct order of magnitude, and further observations at similar low-Froude numbers are needed in order to distinguish between them. In Arneborg et al. (2006) the present data set including the microstructure data presented below is used in combination with a numerical turbulence model to obtain a new relation between entrainment, Froude number and Ekman number.

5.3. Microstructure

Exemplarily for the turbulent mixing of the saline water inflow along its way to the Baltic basins, microstructure and current profiles were taken from the anchored vessel north of Kriegers Shoal. A loosely tethered free-falling microstructure (MST) profiler was used to measure current shear and temperature fluctuations on millimetre vertical

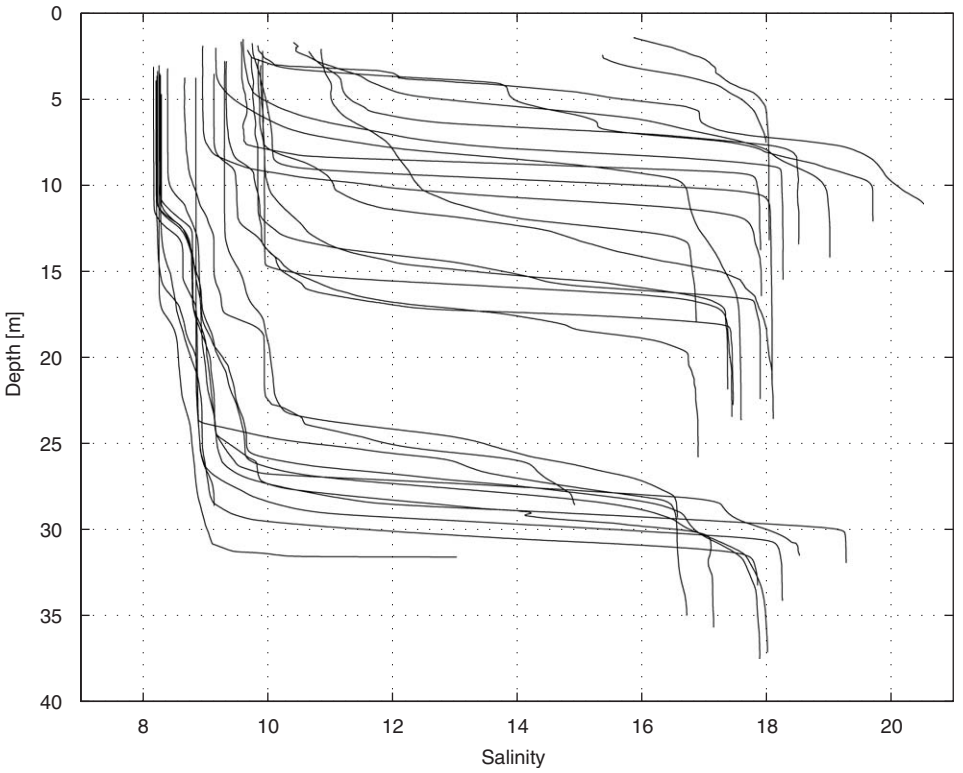

Fig. 11. Salinity profiles from 18:00, February 4 to 13:00, February 6 in the region from the Sound to north of Kriegers Shoal.

scales. The vertical resolution of the vessel mounted 600 kHz ADCP was set to 1 m. Fig. 12 shows the time series of the vertical stratification, the current, and the dissipation rate of turbulent kinetic energy, which are characterized by strong current shear and an abrupt transition from low to high dissipation rates at the depth of the pycnocline at 27 m. While surface water with salinity 8–10 slowly drifts to the west, the bottom layer has eastward velocities of more than 0.6 m/s. The initial salinity in the bottom plume increases from 17.5 to more than 20. Except for the first 3–4 h, dissipation rates of 10^{-7}–10^{-9} W kg^{-1} are observed in the layer from 10 m down to the pycnocline. The dissipation rates within the gravity current below are on the order of 10^{-5} W kg^{-1}. Similar dissipation rates were found only in the mixed layer at the surface, especially during the last 3 h, when the wind speed had increased from 5 to 10 m s^{-1}.

For the determination of eddy diffusivity, the indirect method of Osborn (1980) is usually applied, which calculates eddy diffusivity of mass by the quotient of dissipation rate ε and stability N^2,

$$k_\rho = \gamma \frac{\varepsilon}{N^2}, \tag{8}$$

where γ is the mixing efficiency which quantifies the ratio of the buoyancy flux and the rate of dissipation. In Osborn's model a constant value of 0.2 is often assumed for γ, although it has been shown that the efficiency is not constant. (see e.g. Oakey, 1982; Ruddick et al., 1997). Barry et al. (2001) and Shih et al. (2005) emphasized that γ strongly depends on the buoyancy Reynolds number quantifying turbulence intensity (see Gargett, 1988)

$$\mathrm{Re_b} = \frac{\varepsilon}{\nu N^2}, \tag{9}$$

where ν is the kinematic viscosity.

Shih et al. (2005) pointed out that Osborn's method (8) to estimate the diapycnal diffusivity of density, k_ρ, by means of a constant mixing efficiency $\gamma = 0.2$ has only a narrow range of validity where $7 < Re_b < 100$. In this paper we will use the approach of Shih et al. (2005) who suggest to estimate the turbulent diffusivity of mass by means of the turbulence intensity

$$k_\rho = 2\nu \left(\frac{\varepsilon}{\nu N^2} \right)^{1/2} \tag{10}$$

for the energetic regime $Re_b > 100$.

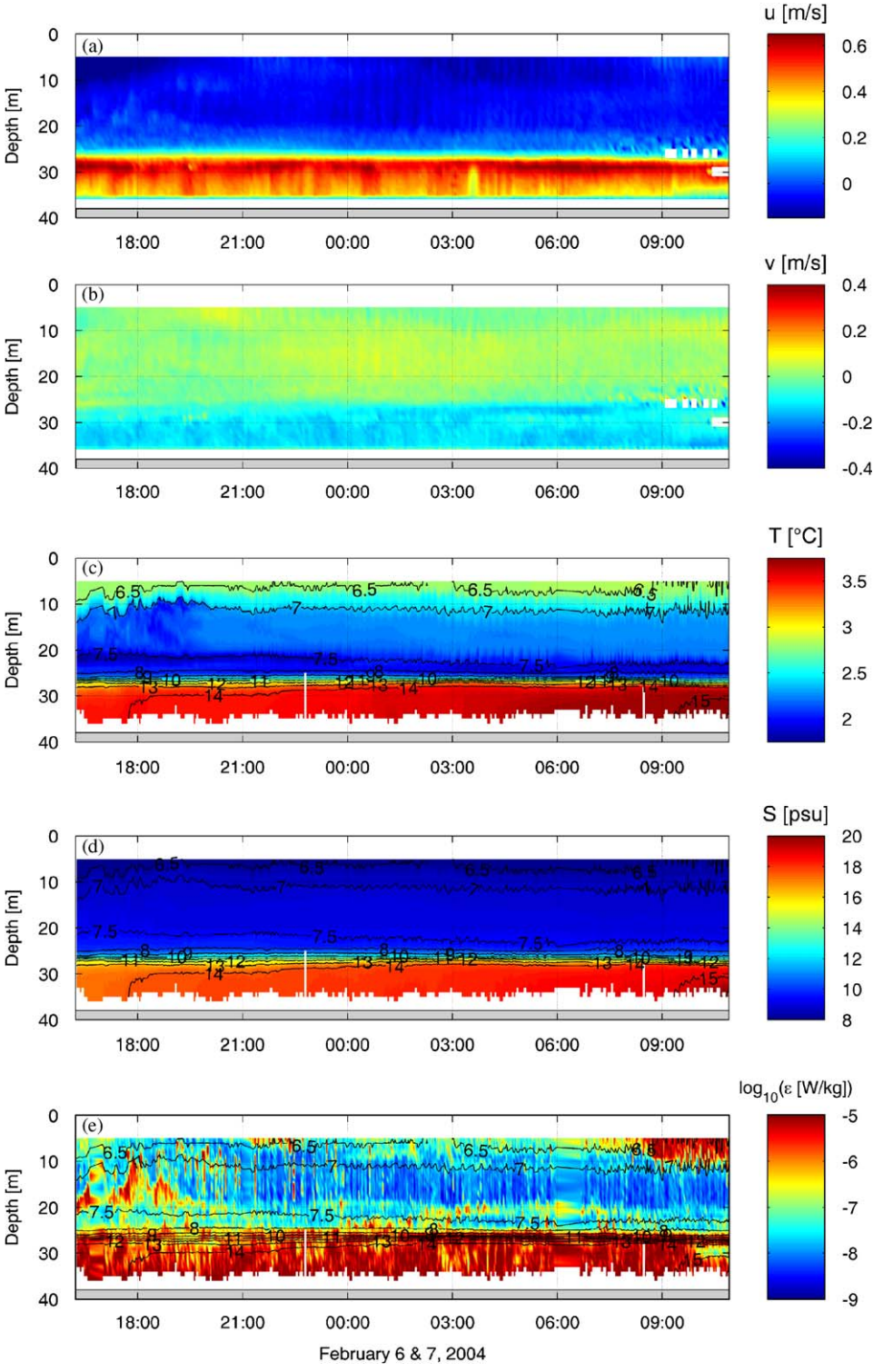

Fig. 12. Observations at anchor station north of Kriegers shoal, showing (a) east and (b) north velocity components from vessel-mounted ADCP, (c) temperature, (d) salinity and (e) dissipation rate of turbulent kinetic energy measured simultaneously with a free-falling MST-Profiler. Empty space above and below measurement data is due to blanking delay and side lobe interference and to the requirement of uniform MST profiler sinking. Contour lines denote density anomaly from 6.5 to 15 kg m^{-3}.

The gradient Richardson number

$$Ri = \frac{N^2}{\left(\partial U/\partial z\right)^2} \tag{11}$$

was estimated by combining density profiles measured with the MST profiler and shear profiles derived from the ADCP measurements. Decreasing Richardson numbers are often related to increasing mixing rates. $Ri < 0.25$ is the necessary condition for turbulent mixing due to the vertical shear.

Mean profiles of various parameters and their spread are shown in Fig. 13. By means of the turbulence intensity (Fig. 13d) and the eddy diffusivity (Fig. 13e) the water column can be subdivided into four different turbulence regimes. The highest Re_b from 10^5 beyond 10^6 occurs close to the surface and near the bottom. With $Re_b > 200$ turbulence is isotropic. In the layer between 20 and 28 m depth, where $Re_b < 200$, turbulence is expected to be anisotropic (Gargett et al., 1984; Gregg and Sanford, 1988; Yamazaki and Osborn, 1990).

Direct comparison of the mean vertical profiles of the eddy diffusivity (Fig. 13f) calculated after Shih et al. (2005) and after Osborn (1980) reveals a small depth range of coincidence for buoyancy Reynolds numbers around 200. In the remaining water column, the discrepancies between both models

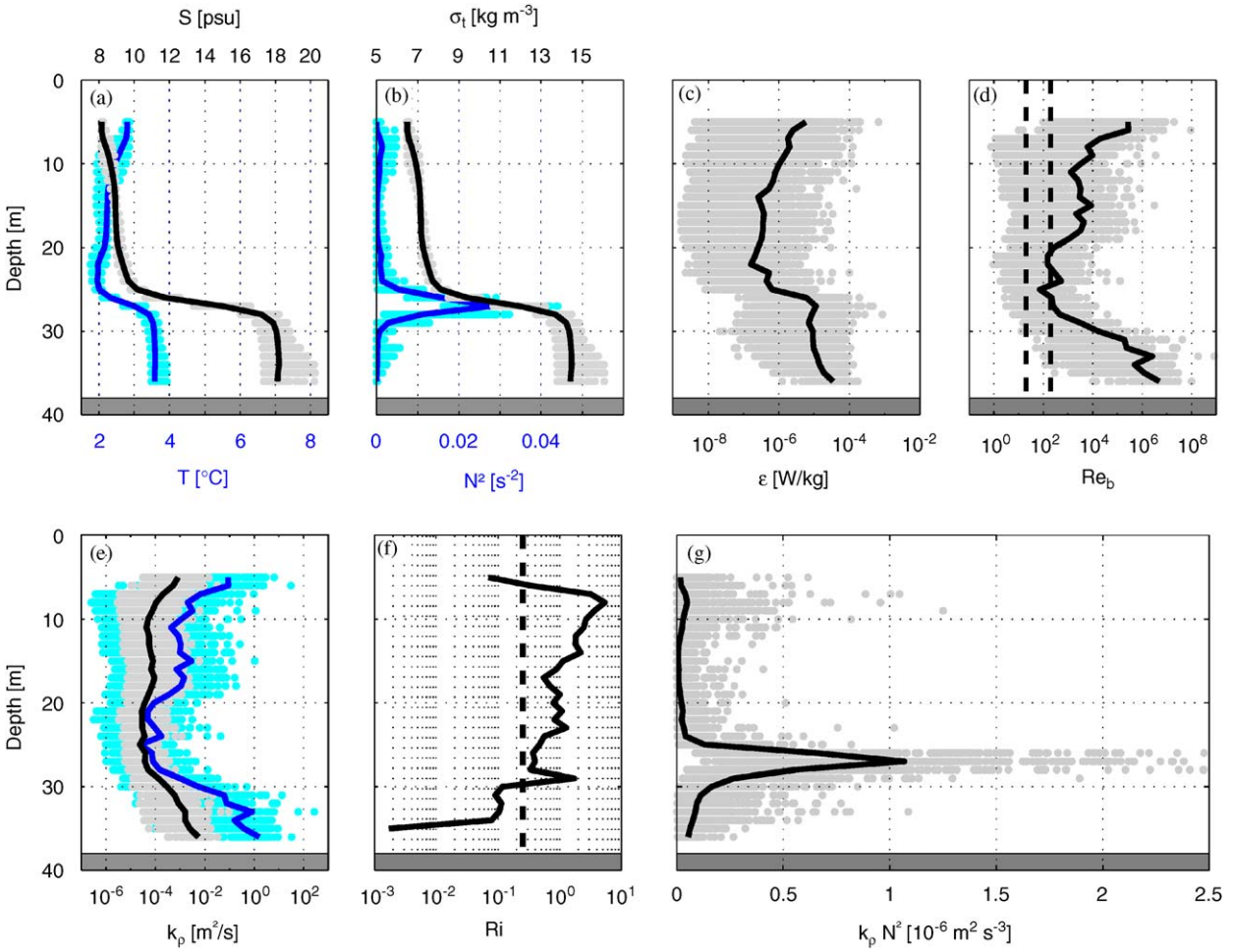

Fig. 13. Mean vertical profiles of 1 m averages during the long-term anchor station north of Kriegers Shoal: (a) temperature T (blue) and salinity S (black); (b) density anomaly σ_t (black) and stability N^2 (blue), (c) dissipation rate ε of the turbulent kinetic energy, (d) buoyancy Reynolds number Re_b, (e) eddy diffusivity k_ρ of mass after Shih et al. (2005) (black) and after Osborn (1980) (blue), (f) gradient Richardson number Ri, and (g) buoyancy flux. The figure includes as grey or cyan background, respectively, the total amount of measurements. The vertical dashed lines in (d) mark the upper limit of turbulent regimes defined by the buoyancy Reynolds numbers $Re_b = 20$and 200. The dashed line in (f) marks the critical gradient Richardson number $Ri = 0.25$.

increase with increasing turbulence intensity. Osborn's model yields higher eddy diffusivities by one order of magnitude in the depth range between 10 and 20 m and by two orders of magnitude in the near surface and bottom layers. While the resultant values after Osborn greatly overestimate k_ρ, diffusivities after Shih et al. amounting to more than $10^{-3}\,m^2\,s^{-1}$ near the bottom are very large but not unusual. Under similar environmental conditions at a tidal plume front of a river outflow, Orton and Jay (2005) observed mean dissipation rates and mean eddy diffusivities of the same order of magnitude.

The gradient Richardson number shown in Fig. 13f gradually decreases from its maximum value of 4 below the wind mixed layer to 0.3 at the lower margin of the pycnocline. From 30 m downwards values below the critical Ri of $\frac{1}{4}$ indicate that the necessary condition for the generation of turbulence was fulfilled. They are in reasonable agreement with the high dissipation rates and the high turbulence intensities found below 30 m. Buoyancy fluxes $N^2 \cdot k_\rho$ of Fig. 13(g) were calculated from k_ρ profiles after Shih et al. (grey scatter points in Fig. 13e) and related profiles of N^2 (cyan scatter points in Fig. 13b). The scatter of the buoyancy flux fills a wide range. The mean buoyancy flux represented by the bold line profile in Fig. 13(g) decreases linearly towards zero at the bottom, as expected for an almost homogeneous bottom boundary layer. The peak in the halocline indicates that the mixing there tends to expand the vertical extent of the halocline at the expense of the more homogeneous layers above and below.

6. Inflow of Darss Sill water

On the long-term average only one quarter of the total inflow to the Baltic Sea comes from the Sound, the majority takes the path through the Great Belt, the Mecklenburg Bight and over the Darss Sill (Nielsen, 2001). The path from the Kattegat to the Arkona Sea through the Great Belt is more than four times longer than through the Sound. While the latter can be completely flushed by a unidirectional current in less than two days, surface water from the Arkona Sea streaming through the Great Belt with an average speed of $0.5\,m\,s^{-1}$ needs a full week before it arrives in the Kattegat. Vice versa in an inflow situation it takes the same amount of time for the surface salinity front to move from the Kattegat to the Darss Sill (Fischer and Matthäus, 1996). Only after several days of strong inflow, Kattegat water with salinity of 18 or more can be expected to arrive in the Arkona Sea.

On the other hand, the Belt Sea and the Western Baltic act as a buffer and mixing vessel for salty water from the Kattegat and fresher water from the Baltic Proper. During winter and spring 2004 salinity at 13 m depth at Kiel lighthouse decreased gradually from 22 to 14; at the MARNET station in the Fehmarn Belt salinity at 23 m depth was close to 20 during the cruise period from January 27 to February 12, at 6 m depth salinity increased from 13 to 20 during the same period due to enhanced vertical mixing (BSH, 2005).

On January 27 a bottom layer with salinity 18 fills the Kadet Trench up to the pycnocline at about 15 m depth. It has different T–S-characteristics but the same density as the bottom water in the Arkona Basin. The two-layer stratification extends to the east over the Darss Sill and is manifested in the salinity records of the Darss Sill MARNET station (Fig. 14), except for a couple of hours on January 29. The surface layer consists of Baltic surface water with salinity 8–9. Baroclinic overflow of bottom water over the Darss Sill can replace a layer of old bottom water in the Arkona Basin and, under favourite conditions, even produce a change of deep water properties in the Gotland Basin (Feistel et al., 2003, 2004). At the end of January 2004, however, the interface between surface and bottom layer was too deep for a significant overflow. The thin bottom layer on Darss Sill was modified by intrusion, so that the small amount of overflow water, which was detected at 54°45′N, 13°E on January 28, had been diluted to salinity 15 already.

By the end of January an increasing wind from westerly directions caused mixing of the water column in the shallow parts of the Mecklenburg Bight and on the Darss Sill. Between February 2 and 6, the main period of the inflow, the water column at the Darss Sill station was nearly homogeneously mixed with salinity increasing from 10 to 12 (Fig. 14). After that period, when the forcing declined, the salinity of the surface layer remained at the high level until February 10 when it dropped, whereas at the bottom higher salinity water arriving from the western Baltic re-established the two-layer stratified system.

The mixed water from the Darss Sill, which is much colder and more saline than Baltic surface water, shows up in a CTD section and a CTD chain tow of February 8 and 9 as a layer between 20 and 35 m depth. In the first panel on the right, Fig. 15

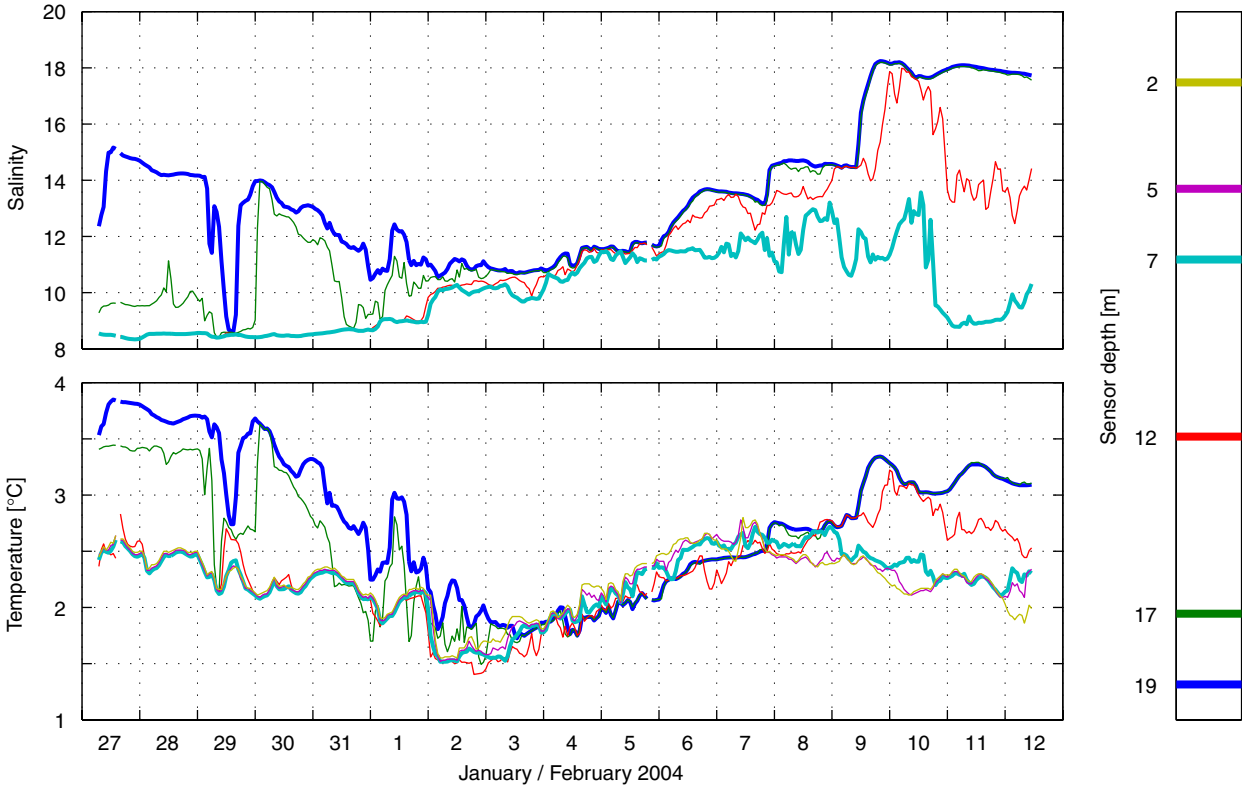

Fig. 14. Salinity at various depths (7, 12, 17, 19 m) at MARNET station Darss Sill.

shows the salinity section obtained from CTD stations between Rügen and a position east of Kriegers Shoal. The Darss Sill water is contained in the dome-shaped structure.

The CTD chain track enters the current band of Darss Sill water 18 km west of the corner point B. Temperature and salinity are displayed in the second and third panel of Fig. 15, respectively. Data were acquired by 81 CTD sensors with 0.5 m spacing at 2 s sampling rate (Sellschopp, 1997). For the compilation of Fig. 15 data were horizontally averaged over 1 min, equivalent to 60–160 m of on-track distance depending on the tow speed over ground.

The eastern and northern current components measured by the ship-borne ADCP are given in the fourth and fifth panel of Fig. 15. Data gaps below 25-m depth are again due to the limited range of the 600 kHz ADCP. A strong eastern current carries Darss Sill water along the southern basin slope. Current speed is about 70 cm s^{-1}. Few kilometres after the tow track leaves the southern rim, the ship-borne ADCP shows a current veering to north. This means that part of the flow circulates back in a cyclonic eddy in the western part of the Arkona Basin. Eddies separating from the northern cape of Rügen have also been observed in the past (Lass et al., 2005).

7. Outflow through the Bornholm Gate

On February 10, a section of 10 CTD casts was performed across the Bornholm Gate from Bornholm in the south-east towards the Swedish coast in the north-west (Fig. 16). On this section, only old Arkona bottom water was observed, and water with salinity more than 12 was only seen at the bottom 10 m of the two deepest casts. Since the bottom water is out of reach of the ship-mounted ADCP, due to the reasons mentioned above, we will estimate the outflow from the Arkona Basin using geostrophic theory. As at Kriegers Shoal, the dense water is seen to lean against the southern coast. However, this case is less straightforward, due to the bad resolution of the CTD casts relative to the topography. If we assume that the isopycnal slopes can be represented by the slope of the salinity 12 isoline (Fig. 16), we can obtain a rough estimate of

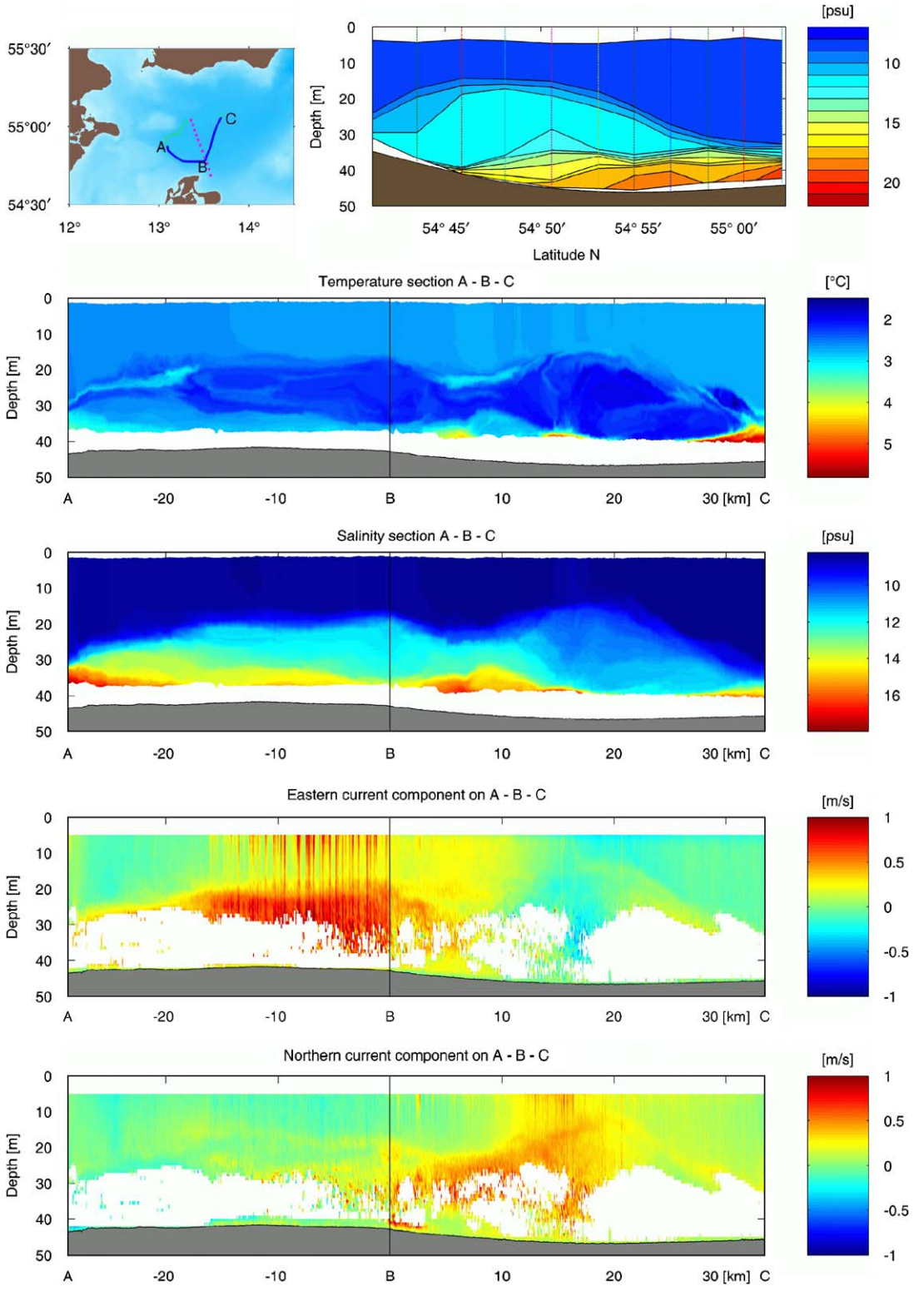

Fig. 15. Darss Sill water with salinity 11–13 in the Arkona Basin. First panel: map of CTD stations and CTD chain track on February 8 and 9 (left) and salinity section obtained from 11 stations (right). Second and third panel: temperature and salinity along the tow track from A to C. Fourth and fifth panel: eastern and northern components of the current along the tow track. Below 30 m depth most values are missing because of the limited range of the 600 kHz ADCP.

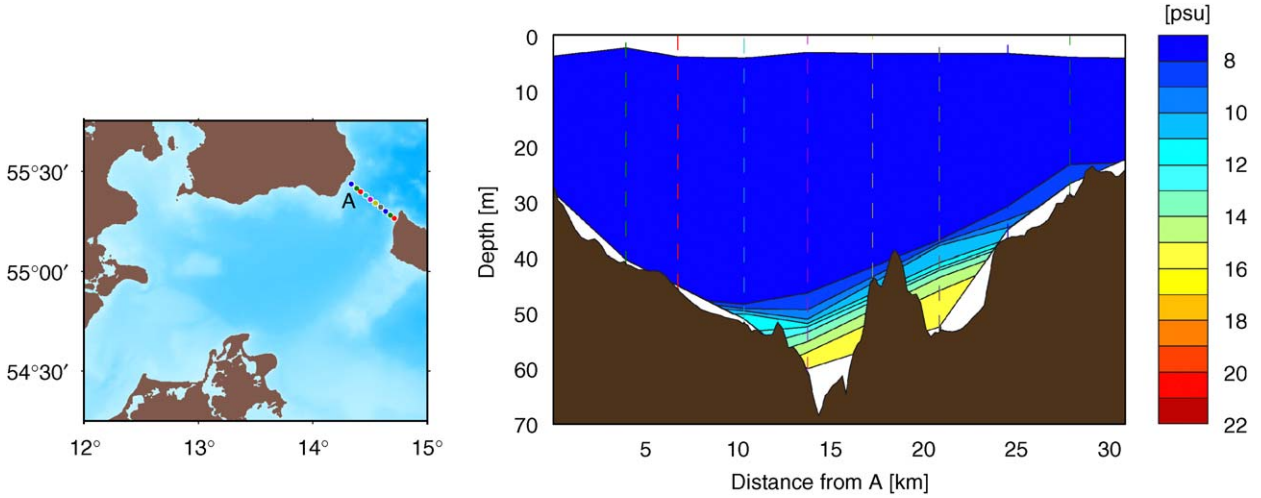

Fig. 16. Salinity cross-section from NW to SE at the Bornholm Gate. At each station the excess salinity (S–S_0) is shown, where $S_0 = 7.6$. The geostrophic current was calculated from slope of the salinity 12 contour.

the bottom layer velocities from

$$U = -g'/f \cdot \partial\eta/\partial y, \tag{12}$$

where $g' = g\beta(S_b - S_0)$ is the reduced gravity, f is the Coriolis parameter, and $\partial\eta/\partial y$ is the cross-channel isopycnal slope. With $\beta \approx 0.0008$, $S_b = 15$, and $S_0 = 7.6$, the reduced gravity is $g' = 0.058\,\mathrm{m\,s^{-2}}$. The slope of the isohaline is $\partial\eta/\partial y = 0.0015$, which means that the geostrophic velocity of the bottom layer is $U = 0.73\,\mathrm{m\,s^{-1}}$. The cross-sectional area below the salinity 12 contour is $83\,000\,\mathrm{m^2}$, which means that the total outflow is around $Q = 61\,000\,\mathrm{m^3\,s^{-1}}$.

On February 10 the inflow from the Sound has slackened and turned to oscillation. The outflow through the Bornholm Gate cannot be directly compared to the inflow from the western sills on the same date. For a period of five days ending on February 8 the average inflow of high salinity water through the Sound had been $30\,000\,\mathrm{m^3\,s^{-1}}$. During the same period moderately saline (salinity 12) water, the quantity of which should have been three times as much, came from the Darss Sill. It has not arrived yet at Bornholm Gate on February 10. Considering these two sources of the buffering Arkona Sea, the calculated magnitude of the outflow through Bornholm Gate looks reasonable.

8. Summary

For the first time a ship survey in the Arkona Sea covered the period before, during and after a medium-size inflow of saline water in winter. After several weeks of rest or oscillations with periods too short to flush the connections between Kattegat and Arkona Sea, all higher salinity water has left the shallower parts northwest of Kriegers Shoal. The halocline separating Baltic surface water with salinities around 8.5 and bottom water with salinity in excess of 15 lies at 35–40 m depth, about 5 m above the bottom of the Arkona Basin. Temperature fine structure in the halocline and above witnesses various inflows in the distant or nearer past.

When saline water arrives through the Sound, it spills down the slope towards Kriegers Shoal. For the medium-size inflow of February 2004 it was observed that the greater portion proceeds along the steepest path north of Kriegers Shoal rather than along the isobaths at the slope of the Darss Sill, indicating that bottom friction is a first-order dynamical process. By its lower temperature the new inflow water was easily distinguished from the old bottom water. The advancement of the inflow forefront and the retreat of older bottom water as observed a few days after the inflow began, also shows that the deepest parts of the basin are flooded in an early stage of the event.

Current velocities of the order $0.5\,\mathrm{m\,s^{-1}}$ and up to $1\,\mathrm{m\,s^{-1}}$ were observed in the saline water layer in the southern Sound, in the branches north and west of Kriegers Shoal and in Bornholm Gate. Pycnoclines showed geostrophic balance in the transverse current direction. North of Kriegers Shoal the

densest bottom water was found on the left side of the current, probably compelled by Ekman veering. Another strong current setting east along the coast of Rügen consisted of water from the Darss Sill, a mixture of Baltic surface water and saline bottom water which had been present in the bottom layer of the Mecklenburg Bight before.

Turbulence measurements showed high dissipation rates in the bottom plume and the pycnocline north of Kriegers Shoal. Eddy diffusivity is large except within the depth range of the pynocline and directly above and very large in the bottom plume. Estimates of entrainment of surface water into the bottom plume are consistent with other findings in the literature.

The measurements in the Arkona Sea were performed as a precursor to the QUANTAS project (Quantification of Water Mass Transformations in the Arkona Sea: Natural Processes and Anthropogenic Influences). This paper is complemented by a paper on numerical modelling for the same period.

Acknowledgements

The excellent preparedness and professionalism of the crew of the multi-purpose vessel Helmsand from the Wehrtechnische Dienststelle 71 in Eckernförde is highly appreciated.

The QuantAS related work at IOW has been kindly supported by The German Federal Ministry for the Environment, Nature Protection and Nuclear Safety and the German Research Foundation.

Lars Arneborg was supported by the Swedish Research Counsel.

The provision of monitoring data by Sveriges Meteorologiska och Hydrologiska Institut and the Danish Farvandsvaesenet is highly appreciated.

The German part of Baltic Monitoring Programme (COMBINE) and stations of the German Marine Monitoring Network (MARNET) in the Baltic Sea are conducted by the Baltic Sea Research Institute Warnemünde (IOW) on behalf of Bundesamt für Seeschifffahrt and Hydrographie (BSH), financed by the Bundesministerium für Verkehr, Bau- und Wohnungswesen (BMVBW).

References

Arneborg, L., Erlandsson, C.P., Liljebladh, B., Stigebrandt, A., 2004. The rate of inflow and mixing during deep-water renewal in a sill fjord. Limnology and Oceanography 49, 768–777.

Arneborg, L., Fiekas, V., Umlauf, L., Burchard, H., 2006. Gravity current dynamics and entrainment—a process study based on observations in the Arkona Basin. Journal of Physical Oceanography, revision submitted for publication.

Barry, M.E., Ivey, G.N., Winters, K.B., Imberger, J., 2001. Laboratory experiments on diapycnal mixing in stratified fluids. 'Aha Huliko'a Hawaiian Winter Workshop, 145–151.

Burchard, H., Lass, H.U., Mohrholz, V., Umlauf, L., Sellschopp, J., Fiekas, V., Bolding, K., Arneborg, L., 2005. Dynamics of medium-intensity dense water plumes in the Arkona Basin, Western Baltic Sea. Ocean Dynamics 55, 391–402.

BSH (Bundesamt für Seeschiffahrt und Hydrographie), 2005, MARNET-Messnetz, 〈http://www.bsh.de/de/Meeresdaten/Beobachtungen/MARNET-Messnetz/index.jsp〉.

Cenedese, C., Whitehead, J.A., Ascarelli, T.A., Ohiwa, M., 2004. A dense current flowing down a sloping bottom in a rotating fluid. Journal of Physical Oceanography 34, 188–203.

Ehlin, U., Mattison, I., Zachrisson, G., 1974. Computer based calculations of volume of the Baltic area. Proceedings of the Ninth Conference of Baltic Oceanographers, Kiel. 17–20 April 1974, pp. 114–128.

Feistel, R., Nausch, G., Matthäus, W., Hagen, E., 2003. Temporal and spatial evolution of Baltic deep water renewal in spring 2003. Oceanologia 45 (4), 623–642.

Feistel, R., Nausch, G., Heene, T., Piechura, J., Hagen, E., 2004. Evidence for a warm water inflow into the Baltic Proper in summer 2003. Oceanologia 46 (4), 581–598.

Fischer, H., Matthäus, W., 1996. The importance of the Drodgen Sill in the Sound for major Baltic inflows. Journal of Marine Systematics 9, 137–157.

Gargett, A.E., 1988. The scaling of turbulence in the presence of stable stratification. Journal of Geophysical Research 93, 5021–5036.

Gargett, A.E., Osborn, T.R., Nasmyth, P., 1984. Local isotropy and the decay of turbulence in a stratified fluid. Journal of Fluid Mechanics 144, 231–280.

Green, M., Stigebrandt, A., 2002. Instrument-induced linear flow resistance in Öresund. Continental Shelf Research 22, 435–444.

Gregg, M.C., Sanford, T.B., 1988. The dependence of turbulent dissipation on stratification in a diffusively stable thermocline. Journal of Geophysical Research 93, 12381–12392.

Gustafsson, B.G., Andersson, H.C., 2001. Modeling the exchange of the Baltic Sea from the meridional atmospheric difference across the North Sea. Journal of Geophysical Research 106, 19731–19744.

Jacobsen, T.S., 1980. Sea water exchange of the Baltic, measurements and methods. Belt Project Report, 106pp. National Agency of Environmental Protection. Copenhagen.

Jakobsen, F., Lintrup, M.J., Steen Møller, J., 1997. Observations of the specific resistance in Öresund. Nordic Hydrology 28, 217–232.

Lass, H.U., Mohrholz, V., 2003. On dynamics and mixing of inflowing saltwater in the Arkona Sea. Journal of Geophysical Research 108 (C2), 3042.

Lass, H.U., Mohrholz, V., Seifert, T., 2002. On the pathways and mixing of salt-water plumes in the Arkona Sea. Meereswissenschaftliche Berichte (Marine Science Reports) No. 54, pp. 38–54, Institut für Ostseeforschung Warnemünde.

Lass, H.U., Mohrholz, V., Seifert, T., 2005. On pathways and residence time of saltwater plumes in the Arkona Sea. Journal of Geophysical Research 110, 24.

Liljebladh, B., Stigebrandt, A., 1996. Observations of the deepwater flow into the Baltic Sea. Journal of Geophysical Research 101, 8895–8911.

Matthäus, W., Franck, H., 1992. Characteristics of major Baltic inflows—a statistical analysis. Continental Shelf Research 12, 1375–1400.

Nielsen, M.H., 2001. Internal hydraulic control in the Northern Öresund. Journal of Geophysical Research 106, 14055–14068.

Oakey, N.S., 1982. Determination of the rate of dissipation of turbulent energy from simultaneous temperature and velocity shear microstructure measurements. Journal of Physical Oceanography 12, 256–271.

Osborn, T.R., 1980. Estimates of the local rate of vertical diffusion from dissipation measurements. Journal of Physical Oceanography 10, 83–89.

Orton, P.M., Jay, D.A., 2005. Observations at the tidal plume front of a high-volume river outflow. Geophysical Research Letters 32, L11605.

Pedersen, F.B., 1980. A monograph on turbulent entrainment and friction in two-layer stratified flow. Ph.D. Thesis, Series Paper 25, IHHE, DTU, Lyngby, Denmark, 397pp.

RDASH (Royal Danish Administration of Navigation and Hydrography), 2004. Oceanography Observations. 〈http://www.frv.dk/en/ifm/oceanografi/oceanografi.htm〉.

Ruddick, B., Walsh, D., Oakey, N., 1997. Variations in apparent mixing efficiency in the North Atlantic Central Water. Journal of Physical Oceanography 27, 2589–2605.

Sellschopp, J., 1997. A towed CTD chain for two-dimensional high resolution hydrography. Deep-Sea-Research I 44, 147–165.

Shih, L.H., Koseff, J.R., Ivey, G.N., Ferziger, J.H., 2005. Parameterization of turbulent fluxes and scales using homogeneous sheared stably stratified turbulence simulations. Journal of Fluid Mechanics 525, 193–214.

SMHI (Swedish Meteorological and Hydrographic Institute), 2006. Observations. The Sound. 〈http://www.smhi.se/hfa_coord/BOOS/Sound.html〉.

Stigebrandt, A., 1987. A model for the vertical circulation in the Baltic deep water. Journal of Physical Oceanography 17, 1772–1785.

Wåhlin, A.K., Cenedese, C., 2006. How entraining density currents influence the ocean stratification. Deep-Sea Research II 53, 172–193.

Yamazaki, H., Osborn, T., 1990. Dissipation estimates for stratified turbulence. Journal of Geophysical Research 95, 9739–9744.